Histone H4 post-translational modifications in chordate mitotic and endoreduplicative cell cycles

ARTICLE *in* JOURNAL OF CELLULAR BIOCHEMISTRY · AUGUST 2005

Impact Factor: 3.26 · DOI: 10.1002/jcb.20416 · Source: PubMed

3 AUTHORS, INCLUDING:

Fabio Spada
Ludwig-Maximilians-University of Munich
41 PUBLICATIONS **1,422** CITATIONS
SEE PROFILE

Eric M Thompson
University of Bergen
86 PUBLICATIONS **2,010** CITATIONS
SEE PROFILE

Journal of Cellular Biochemistry 95:885–901 (2005)

Histone H4 Post-Translational Modifications in Chordate Mitotic and Endoreduplicative Cell Cycles

Fabio Spada,* Mariacristina Chioda, and Eric M. Thompson*

Sars International Centre for Marine Molecular Biology, Bergen High Technology Centre, Thormølensgt. 55, N-5008 Bergen, Norway

Abstract Histone post-translational modifications mark distinct structural and functional chromatin states but little is known of their involvement in the progression of different cell cycle types across phylogeny. We compared temporal and spatial dynamics of histone H4 post-translational modifications during both mitotic and endoreduplicative cycles of the urochordate, *Oikopleura dioica*, and proliferating mammalian cells. Endocycling cells showed no signs of chromosome condensation or entry into mitosis. They exhibited an evolution of replication patterns indicative of reduced chromatin compartmentalization relative to proliferating mammalian cells. In the latter cells, published cell cycle profiles of histone H4 acetylated at lysine 16 (H4AcK16) or dimethylated at lysine 20 ($H4Me_2K20$) are disputed. Our results, using different, widely used H4AcK16 antibodies, revealed significant antibody-specific discrepancies in spatial and temporal cell cycle regulation of this modification, with repercussions for interpretation of previous immunofluorescence and immunoprecipitation data based on these reagents. On the other hand, three different antibodies to $H4Me_2K20$ revealed similar cell cycle profiles of this modification that were conserved throughout the mitotic cell cycle in urochordate and mammalian cells, with accumulation at mitosis and a decrease during S-phase. $H4Me_2K20$ also cycled in endocycles, indicating that dynamics of this modification are not strictly constrained by the mitotic phase of the cell cycle and suggesting additional roles during G- and S-phase progression. This article contains Supplementary Material available at http://www.mrw.interscience.wiley.com/suppmat/0730-2312/suppmat/2005/95/spada.html. J. Cell. Biochem. 95: 885–901, 2005. © 2005 Wiley-Liss, Inc.

Key words: histone methyltransferase; histone acetylation; histone code; urochordate; appendicularia; endocycle; oikoplastic epithelium; replication pattern; chromatin

Post-translational modifications of core histones are thought to constitute a "histone code" specifiying functional states of chromatin with respect to processes such as transcription and replication [Jenuwein and Allis, 2001] and may propagate such states through multiple rounds of cell division [Turner, 2000; Lachner et al., 2003]. As part of this code, acetylation at specific lysine residues of core histones in regulatory sequences is involved in determining transcriptional activity [Agalioti et al., 2002]. However, local acetylation accounts for a small fraction of total acetylated chromatin in the genome [Turner, 2000; Forsberg and Bresnick, 2001]. A more global role for acetylation in establishing patterns of chromatin structure and function is observed at the level of whole chromosomes and genomes. The N-terminal tail of histone H4 can be acetylated at lysine residues 5, 8, 12, and 16 (K5-16). Most metazoans, plants and the budding yeast *S. cerevisiae* display a preferred, but not absolute order in the steady state of acetylation at these four sites, with most monoacetylated isoforms at K16, the diacetylated at K16 and 12 (or 8), and the triacetylated at K16, 12, and 8 or 5 [Turner et al., 1989; Thorne et al., 1990; Waterborg, 1992; Clarke et al., 1993; Belyaev et al., 1996]. These observations led to the idea of an acetylation and deacetylation

Grant sponsor: Norwegian Research Council; Grant number: 146653/431.

Fabio Spada's present address is Department of Biology II, Ludwig Maximilian University, 82152 Planegg-Martinsried, München, Germany.

Mariacristina Chioda's present address is Adolf Butenandt Institut, Molekularbiologie, Schillerstr. 44, 80336 München, Germany.

*Correspondence to: Fabio Spada and Eric M. Thompson, Sars International Centre for Marine Molecular Biology, Bergen High Technology Centre, Thormølensgt. 55, N-5008 Bergen, Norway. E-mail: f.spada@lmu.edu; Eric.Thompson@sars.uib.no

Received 1 November 2004; Accepted 8 December 2004

DOI 10.1002/jcb.20416

cycle of H4 proceeding preferentially and sequentially from K16 to 5 and vice versa. Varying degrees of compartmentalization of acetylated H4 isoforms have been observed in distinct chromatin domains. In *S.cerevisiae*, H4 acetylation at K16 (H4AcK16) is present in euchromatin and depleted in the heterochromatic telomeres and mating type loci [Braunstein et al., 1993, 1996; Suka et al., 2001; Kurdistani and Grunstein, 2003; Kurdistani et al., 2004]. Analogously, mammalian mitotic chromosomes are largely hypoacetylated at all H4 acetylation sites in pericentromeric heterochromatin and in the inactive X chromosome [Jeppesen and Turner, 1993]. This is consistent with a conserved role for the global level of H4 acetylation in distinguishing euchromatin from domains of facultative and constitutive heterochromatin. In addition, acetylation of H4 at K12, 8, and 5 shows progressively sharper banding patterns, while that of K16 has the most uniform pattern along the arms of mammalian chromosomes [Jeppesen and Turner, 1993; Belyaev et al., 1996]. These data suggest that H4AcK16 represents a key step onto which further functional and structural chromatin organization is built by progressive acetylation of H4.

In addition to acetylation at these four positions and methylation at arginine 3, the histone H4 N-terminal tail can be methylated at K20 [Borun et al., 1972]. Recent isolation and characterization of H4K20 methyltransferases in *Drosophila* and mammals and use of antibodies to methylated H4K20 showed that this modification has much in common with methylation at H3K9 [Fang et al., 2002; Nishioka et al., 2002; Schotta et al., 2004]. H4 di- and trimethylated at K20 ($H4Me_2$- and Me_3K20) are abundant in the chromocentre of *Drosophila* polytene chromosomes, and the $H4Me_2K20$ banding pattern does not overlap transcriptionally competent regions identified by the presence of elongating RNA polymerase II and histone H3 methylated at K4, suggesting an association with silent chromatin. While Nishioka et al. showed evidence supporting a negative interplay between H4AcK16 and $H4Me_2K20$, Fang et al. reported essentially opposite results [Fang et al., 2002; Nishioka et al., 2002]. Contrasting data have also been reported on the cell cycle dynamics of $H4Me_2K20$ levels in mammalian cells [Fang et al., 2002; Rice et al., 2002]. Rice et al. also showed a cell cycle profile for H4AcK16 complementary to that of $H4Me_2K20$ in mammalian cells. Thus, the cell cycle dynamics of $H4Me_2K20$ and its interplay with H4AcK16 remain controversial and the roles of these modifications in cell cycle related processes are poorly understood. In particular, the nuclear distribution of these modifications has not been sufficiently characterized with respect to different stages of the cell cycle apart from mammalian mitotic chromosomes. In addition, it is unknown whether these modifications have similar roles in cells undergoing different types of cell cycle and/or in evolutionary divergent organisms.

After rapid embryonic development, cells in most tissues of the pelagic tunicate, *Oikopleura dioica*, stop proliferating and enter endoreduplicative cycles characterized by alternating G- and S-phases. The timing of this developmental switch to endocycles and rates of successive endocycles vary among cell types according to a tightly regulated program [Ganot and Thompson, 2002]. This generates marked differences in cell size, nuclear morphology, and DNA content and drives a tenfold somatic growth over the short 6-day lifespan. Among endocycling tissues, the easily accessible and transparent oikoplastic epithelium is a bilaterally symmetric monolayer that covers the trunk of the animal. Several distinct cellular fields can be clearly recognized within this epithelium, characterized by specific sizes and nuclear morphologies. In contrast to *Drosophila* endocycling tissues (e.g., salivary glands), there is no formation of polytene chromosomes in *O. dioica* nor is there chromosome condensation during the endocycle. DNA replication is asynchronous within the diverse cellular fields of the oikoplastic epithelium but there is a precise bilateral symmetry in the entry and exit from S-phase [Ganot and Thompson, 2002], making this tissue exceptionally well-suited to exploring the in vivo dynamics of cell cycle related histone modifications. *O. dioica* also occupies a key evolutionary position at the transition between invertebrates and vertebrates where there is a gap in information on chromatin epigenetics and dynamics.

In the present study, we examined the temporal and spatial dynamics of H4AcK16 and $H4Me_2K20$ during mitotic and endocycles of *O. dioica* and compared them with those in the mitotic cycle of cultured mammalian cells. With three widely used antibodies against H4AcK16,

we observed complex temporal and spatial patterns of this modification during the cell cycle of both *O. dioica* and mammalian cells. There were, however, significant antibody-specific inconsistencies. On the other hand, three different antibodies to $H4Me_2K20$ yielded identical results consistent with temporal profiles in mammalian cells characterized by Rice et al. [2002], but in disagreement with those proposed by Fang et al. [2002]. A very similar cell cycle profile for $H4Me_2K20$ was observed in *O. dioica* mitotically cycling cells, with accumulation of the modification at mitosis and a decrease during S-phase. Interestingly, a similar cell cycle profile was also observed in *O. dioica* endocycling cells in the complete absence of the mitotic transition.

MATERIALS AND METHODS

Animal and Cell Culture

O. dioica were obtained and cultured as described [Chioda et al., 2004]. NIH3T3 and HeLa S3 cells were cultured in DMEM containing 5 and 10% FCS (Sigma), respectively, in a 5% CO_2 humidified atmosphere at 37°C. HeLa S3 cells were synchronized at the G1/S-phase transition by double thymidine block. NIH3T3 cells were synchronized in early G1 by a nocodazole block (Sigma, 50 ng/ml for 4 h), followed by manual shake off and plating on coverslips in nocodazole-free medium. Cells were fixed (as below) 3 h after release.

Antibodies and Immunoblotting

The following antibodies were from Upstate: RbA (#07-367; [Fang et al., 2002]), RbB (#07-031 [Nishioka et al., 2002]), and MAb (clone 6G7/H4, #05-672 [Nishioka et al., 2002]) to $H4Me_2K20$; rabbit polyclonals to H4AcK16 (U, #07-329; [Suka et al., 2001]), H3Sp28 (#07-145), and H3Sp10 (#06-570 [Hendzel et al., 1997]). Other antibodies to acetylated H4 were from Serotec (AcK16 S, AHP417) or from B.M. Turner (sera R14/16 to Ac16 [Turner et al., 1989], R101/12 to Ac12, R323/8 to Ac8 and R41/5 to Ac5 [White et al., 1999]). Identical results were obtained with different lots of the H4AcK16 S antibody (Serotec). Antibodies against the H4 C-terminus, actin, and cyclin A were from Santa Crutz Biotechnology (sc-8658), Lab Vision (clone ACTN05, Ab-5), and Zymed Laboratories (clone E23, #33-4900), respectively. Modified and unmodified peptides spanning residues 11–24 of histone H4 [GKGGAKRHRKVLRD] were synthesized, purified by RP-HPLC, and quality controlled by mass spectrometry at Alpha Diagnostic International. They were blotted onto nitrocellulose membranes (Hybond-C, Amersham) and loading was controlled by staining with Sypro Ruby Protein Blot Stain (Bio-Rad). Whole cell and *O. dioica* tadpole extracts were separated by SDS–PAGE and blotted onto PVDF membranes (Immobilon-P, Millipore). Blots were blocked with 3% BSA in PBS containing 0.1% Tween 20 (PBT) and incubated with primary antibodies in blocking buffer for 2 h at room temperature (RT). Antibodies on slot blots were detected by ECL (Amersham). Western blots were sequentially subjected to rabbit antibodies to histone modifications detected by ECL and then to antibodies to H4 C-terminus and actin or cyclin A simultaneously, detected with alkaline phosphatase-conjugated secondary antibodies and CDP-Star chemioluminescent substrate (Roche). Rabbit α-H3Sp28 and goat α-H4 C-terminus were detected simultaneously.

Replication Pulse Labeling and Immunofluorescence

O. dioica tadpoles and day 3 juveniles were cultured in a 1 mM solution of either BrdU, CldU, or IdU in seawater containing the standard algal food regime for indicated pulse lengths. In single BrdU pulse experiments, the animals were fixed at the end of the pulse with 4% paraformaldehyde (PFA) in 0.5 M NaCl, 0.1 M MOPS pH 7.5, 0.1% Triton X-100 for 1 h at RT. In double pulse experiments, day 3 animals were pulsed with CldU, chased by transferring them to seawater without thymidine analogs for the indicated time, pulsed again with IdU and fixed as above. In order to expose thymidine analog epitopes samples were treated with 5 U/ml of DNAse I (Worthington) in PBT, 0.5% acetylated BSA (Sigma), and 5 mM $MgCl_2$ for 1 h at RT. This method maximally preserved morphological detail and integrity of protein antigens. Samples were washed with PBT containing 1 mM EDTA (PBTE) and blocked ON at 4°C with 3% acetylated BSA in PBTE. All primary antibody incubations were for 1 week at 4°C in blocking buffer and were followed by post-fixation in 4% PFA in PBTE for 1 h at RT. In single pulse experiments, BrdU was detected with a sheep polyclonal α-BrdU antibody (Abcam) incubated simultaneously with both the rabbit α-H4AcK16 and mouse

monoclonal α-H4Me$_2$K20 antibodies. Alternatively, polyclonal antibodies to either H4AcK16 or H4Me$_2$K20 were used. In double pulse experiments, CldU and IdU were detected by sequential incubations with a rat monoclonal α-BrdU antibody (clone Bu1/75), which reacts with CldU but not with IdU, and a mouse monoclonal α-IdU antibody which binds preferentially to IdU (clone IU-4, both from Accurate Chemicals). The absence of cross-reaction of these antibodies was monitored by staining animals pulsed with only CldU or IdU. Rabbit polyclonal antibodies to either H4AcK16 or H4Me$_2$K20 were present during both incubations. NIH3T3 and HeLa S3 cells were cultured in 50 μM BrdU for 10 min immediately before fixation with 4% PFA in PBS for 10 min. at RT. Cells were permeabilized with 0.5% Triton X-100 in PBS and treated with 10 U/ml of DNAse I in PBT containing 3% BSA and 5 mM $MgCl_2$ for 1 h at 37°C. After washing with 0.1% BSA in PBTE, cells were incubated in 3% BSA/PBTE overnight at 4°C with the combinations of primary antibodies indicated above for single BrdU pulses and no post-fixation was used. Secondary antibodies conjugated with FITC, rhodamine Red-X, or Cy5 were from Jackson Laboratories, and Alexa Fluor 568-conjugated goat α-rabbit was from Molecular Probes. For *O. dioica* samples, secondary antibodies were incubated at 4°C for 1 week, while for mammalian cells incubations were for 2 h at RT. Where indicated, DNA was counterstained with 1 μM TO-PRO-3 (Molecular Probes). All samples were mounted in Vectashield (Vector Laboratories) and images were collected with a Leica TCS-SP confocal microscope equipped with an oil PL APO 63× objective (NA 1.4-0.6) and Leica Confocal Software.

RESULTS

Specificity of α-H4 AcK16 and α-H4 Me$_2$K20 Antibodies

Contrasting data on the profile of H4Me$_2$K20 throughout the mitotic cycle of mammalian cells were previously reported [Fang et al., 2002; Rice et al., 2002]. Different antibodies to H4Me$_2$K20 were used in these studies and it has been proposed that profile discrepancies may have resulted from different antibody affinities with respect to a potential steric hindrance by acetylation at K16 [Turner, 2002]. A relevant observation is that K20 can be dimethylated in all acetylated forms of H4 upon treatment of HeLa cells with butyrate [Fang et al., 2002; Zhang et al., 2002]. The same affinity question applies to antibodies against H4AcK16 with respect to the methylation status of K20. The question of affinities and specificities of the respective antibodies is important in the interpretation of results that have suggested a negative interplay between the two modifications [Nishioka et al., 2002; Rice et al., 2002]. We therefore tested the reactivity of a panel of H4Me$_2$K20 and H4AcK16 antibodies with H4 N-terminal peptides bearing AcK16, Me$_2$K20, or both, by a slot blot assay (Fig. 1). This panel included antibodies used in Nishioka et al. and Rice et al. (subsequently referred to as H4AcK16 S, H4Me$_2$K20 RbA and MAb) and in Fang et al. (α-H4Me$_2$K20 RbB), as well as two additional antibodies to H4AcK16 subsequently referred to as U [Suka et al., 2001] and serum R14/16 [Turner et al., 1989]. All antibodies to H4AcK16 and antibodies H4Me$_2$K20 RbA and MAb bound the doubly modified peptide as efficiently as the peptide containing only their target modification. Antibody H4Me$_2$K20 RbB was previously reported to recognise all acetylated forms of histone H4 [Fang et al., 2002]. However, this was the only antibody that reacted significantly with the unmodified H4 peptide and showed reduced binding to the doubly modified peptide relative to the peptide bearing only the target modification. In our hands H4Me$_2$K20 RbB yielded poor chromatin staining on whole mount *O. dioica* specimens and 3T3 mouse fibroblasts, labeling mainly nucleoli in the latter cells (not shown). In contrast, the other antibodies to H4Me$_2$K20 displayed robust and consistent immunofluorescent staining of chromatin in cultured mammalian cells and *O. dioica* samples (Figs. 2–6). The peptide slot blots indicated that reported discrepancies in the cell cycle profile of H4Me$_2$K20 may in part be due to the different reactivities of antibodies used in those studies, but that the proposed negative interplay between H4AcK16 and H4Me$_2$K20 [Nishioka et al., 2002; Rice et al., 2002] cannot be wholly explained by differential affinity of antibodies to H4 molecules bearing AcK16 and Me$_2$K20 simultaneously.

H4Me$_2$K20 and H4AcK16 Dynamics in *O. dioica* Mitotic and Endocycling Cells

Oikoplastic epithelial cells of *O. dioica* occupying bilaterally symmetric positions undergo

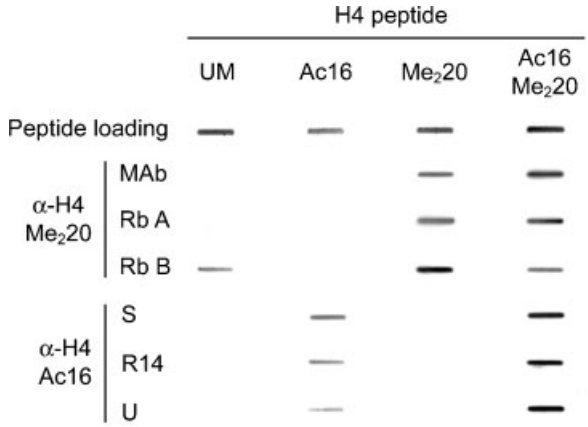

Fig. 1. Antibody specificity. Slot blot assay with synthetic N-terminal peptides (residues 11–24) of histone H4 that were either unmodified (UM), acetylated at lysine 16 (Ac16), dimethylated at lysine 20 ($Me_2$20), or contained both modifications. Serial dilutions of the peptides were loaded on membranes and challenged with mouse monoclonal (MAb) and rabbit polyclonal (RbA and B) antibodies to H4 Me_2K20 and polyclonal antibodies S, U and R14/16 to H4 AcK16. One dilution point of each peptide is shown for each antibody. Peptide loading was controlled by Sypro Ruby protein blot staining as shown in the upper row. Only the α-H4Me_2K20 RbB showed any cross-reaction (unmodified peptide) or a reduction in antigen recognition in the presence of the second peptide modification.

synchronous endocycles, giving rise to symmetrical replication patterns [Ganot and Thompson, 2002]. Therefore, if levels of H4AcK16 and H4Me_2K20 vary according to cell cycle stage, as suggested for cultured mammalian cells [Rice et al., 2002], bilaterally symmetric patterns of these modifications would be predicted across the oikoplastic epithelium. To test this, day 3 animals were cultured in the presence of BrdU for 30–40 min, fixed immediately and immunostained for BrdU, H4Me_2K20, and/or H4AcK16 (Fig. 2). Bilateral symmetry in the patterns of BrdU incorporation and H4Me_2K20 (shown only for the MAb antibody) and H4AcK16 (antiserum S) staining were evident across the epithelium (Fig. 2A,B). Some complementarity in the staining intensity of MAb α-H4Me_2K20 and α-H4AcK16 antiserum S was observed: cells strongly labeled by one antibody were often weakly stained by the other, though a few cells with relatively high levels of both modifications were found. Notably, oikoplastic cells displayed distinct replication patterns, the same range of patterns being observed in diverse fields of oikoplastic cells. Distinct replication patterns were consistently associated with different intensities of α-H4AcK16 S and α-H4Me_2K20 staining. Nuclei with high levels of BrdU incorporation were strongly stained by the α-H4AcK16 S serum, and showed variable, sub-maximal intensity with α-H4Me_2K20 antibodies. Indeed, nuclei with the most intense H4Me_2K20 signals displayed either partial, very limited, or no replication. Essentially identical results were obtained with MAb and RbA α-H4Me_2K20 antibodies, except that the former exhibited higher signal intensities. Single immunostaining with antibodies against H4AcK16 or H4Me_2K20 coupled with the fluorescent DNA dye TO-PRO-3 demonstrated that differences in signal intensity among nuclei were not due to differences in DNA content (Supplementary Fig. 1. Supplementary material for this article is available at http://www.mrw.interscience.wiley.com/suppmat/0730-2312/suppmat/2005/95/spada.html). These results suggested that, as reported for mitotically cycling mammalian cells, H4AcK16 and H4Me_2K20 levels also vary throughout *O. dioica* endocycles despite a complete absence of mitosis, the stage when H4Me_2K20 accumulates in mammalian cells. However, serum R14/16 to H4AcK16 [Turner et al., 1989] showed much more limited variability in its staining intensity of oikoplastic nuclei than serum H4AcK16 S and no correlation was observed with the levels and patterns of BrdU incorporation (Fig. 2C,D).

Mitotically dividing cells of 4 h tadpoles (not shown) and day 3 *O. dioica*, pulsed with BrdU, were also analyzed for cell cycle dynamics of H4AcK16 and H4Me_2K20 (Fig. 3). G-phase cells displayed two combinations with opposite levels of signal from α-H4AcK16 S and α-H4Me_2K20 MAb antibodies. Three major replication patterns were associated with distinct signal levels from the two antibodies: partial and low level BrdU incorporation correlated with strong H4AcK16 S and low H4Me_2K20 signals, broad and strong BrdU incorporation with intermediate signal levels for both antibodies, and patchy, high level BrdU incorporation with strong H4AcK16 S and weak H4Me_2K20 signals. Very similar patterns were present in early embryonic cells (not shown). Similar to observations in endocycling cells, variation in the staining intensity with antiserum R14/16 was more modest and did not consistently correlate with patterns of BrdU incorporation (Fig. 3B).

Formation of highly condensed chromosomes was observed (M in Fig. 3A), but their small size and the absence of typical metaphase

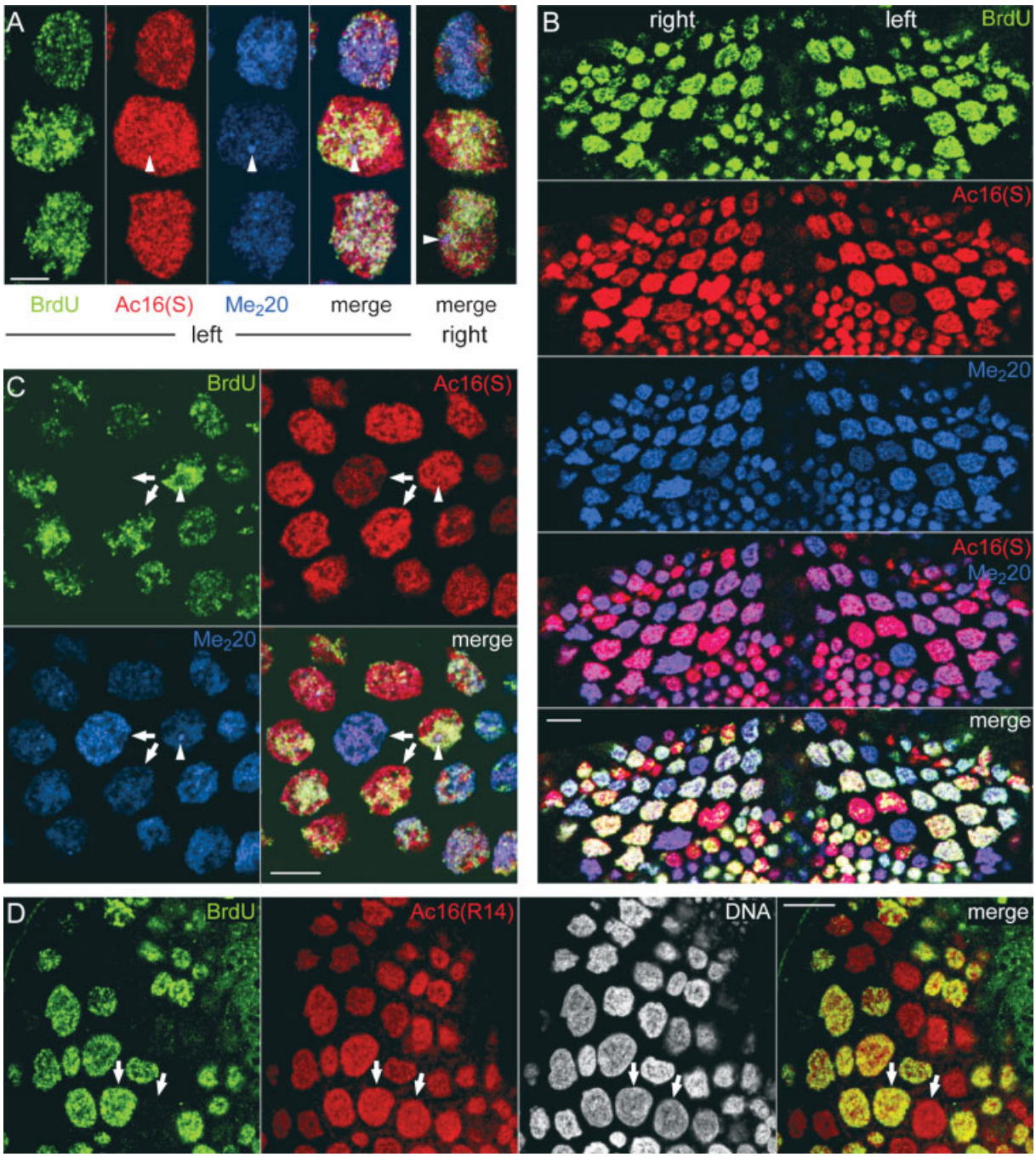

Fig. 2. Variable levels of H4AcK16 and Me_2K20 staining exhibit bilateral symmetry in endocycling nuclei of *Oikopleura dioica*. Day 3 *O. dioica* specimens subjected to a BrdU pulse were immunolabeled for BrdU (green), and with antibodies H4AcK16 S (red) and H4Me2K20 MAb (blue; **A–C**) or with serum H4AcK16 R14 (red) and the DNA fluorescent dye TO-PRO-3 (grayscale; **D**). Single optical sections through the three central giant cells of the field of Eisen (A) and the anterior part of the Fol region (B) show left-right staining symmetry across the dorsal midline. C, D: Single optical sections of the posterior oikoplastic epithelium. Arrows indicate pairs of nuclei with one in S and the other in G phase. These pairs have different staining levels for $H4Me_2K20$ as well as for H4AcK16 revealed by serum S but not for H4AcK16 revealed by serum R14. Arrowheads in (A) and (C) indicate condensed chromatin domains enriched in $H4Me_2K20$. These domains are characterized by enriched levels of $H3Me_{2-3}K9$ and methylated DNA and by depletion of H4AcK8 [Spada et al., 2005].

plates made identification of mitotic stages less straightforward than in mammalian cells. To determine unambiguously the levels of $H4Me_2K20$ associated with *O. dioica* mitotic chromatin, samples were double labeled with antibodies to $H4Me_2K20$ (MAb) and H3 phosphorylated at serine 28 (H3pS28), a modification detected in mitotic chromosomes of mammalian cells from prophase to anaphase [Goto et al., 1999, 2002]. Condensed chromosomes of *O. dioica* were characterized by high levels of both modifications (Fig. 3C). Essentially identical results were obtained with an antibody to H3 phosphorylated at serine 10, which is also highly abundant in mitotic chromatin [Hendzel et al., 1997]. Taken together, these results showed that variations in the levels of $H4Me_2K20$ occur throughout both mitotic and endocycles of *O. dioica*. On the other hand, inconsistent results obtained with different antibodies to H4AcK16 did not allow clear conclusions to be drawn about the cell cycle dynamics of this histone modification in *O. dioica* and raised the same concern about its reported variations during the mammalian mitotic cell cycle.

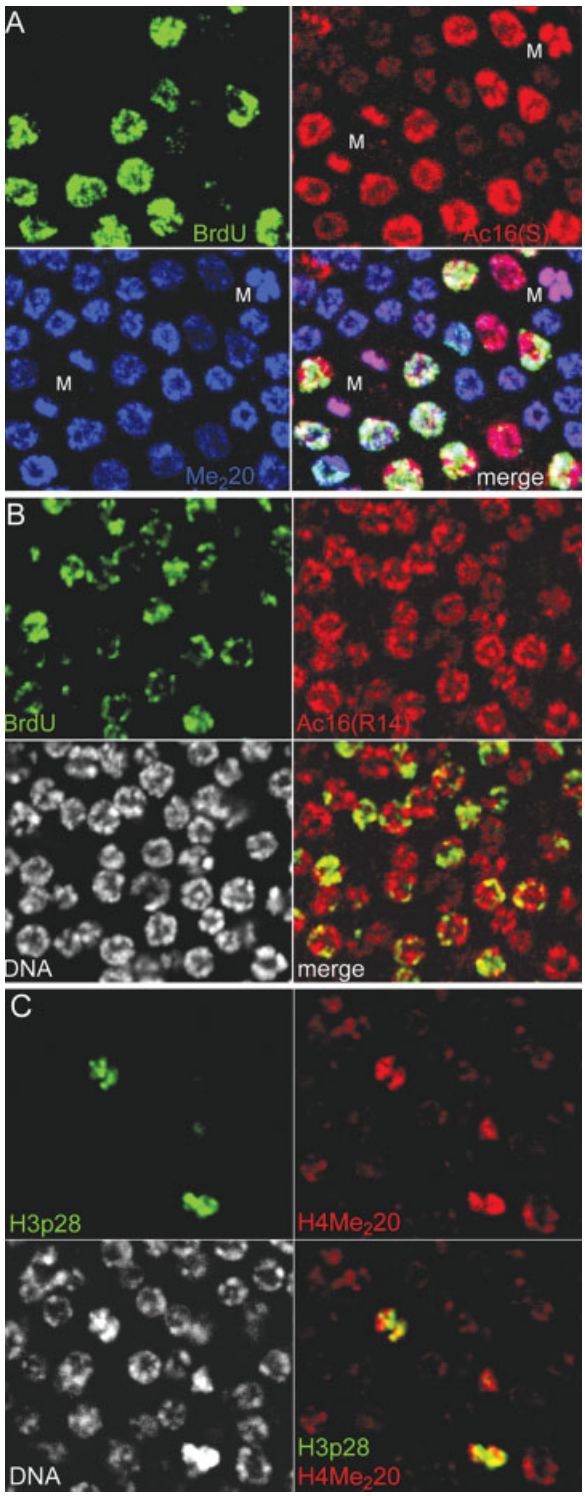

Fig. 3. Different levels of H4AcK16 and $H4Me_2K20$ associate with distinct stages of the mitotic cell cycle in *Oikopleura dioica* endothelial cells. **A–B**: Day 3 specimens were pulsed with BrdU for 30–40 min and simultaneously labeled with antibodies to BrdU (green), H4AcK16 (red) and either with the $H4Me_2K20$ MAb antibody (A; blue) or the DNA dye TO-PRO-3 (B; grayscale). **C**: Mitotic cells and associated levels of $H4Me_2K20$ in day 3 animals were identified by simultaneous labeling with antibodies to H3Sp28 (green) and $H4Me_2K20$ MAb (red). DNA was counterstained with TO-PRO-3 (grayscale). A: It shows a projection of optical sections. Mitotic cells (M) are indicated. B, C: They show single optical sections.

Cell Cycle Dynamics of $H4Me_2K20$ and H4AcK16 in Mammalian Cells

Dynamic and complementary cell cycle profiles of H4AcK16 and $H4Me_2K20$ have been previously revealed by Western blotting of synchronized HeLa cell extracts using serum H4AcK16 S and either the α-$H4Me_2K20$ RbA or MAb antibody [Rice et al., 2002]. These authors found $H4Me_2K20$ to be less abundant from mid S- to G2-phases and to accumulate at mitosis. In contrast, a concurrent study using synchronized HeLa cells and antibody $H4Me_2K20$ RbB showed that $H4Me_2K20$ levels were higher during S-phase and decreased during G2/M-phase [Fang et al., 2002]. These discrepancies and those shown above for signal levels detected with α-H4AcK16 antibodies throughout *O. dioica* mitotic and endocycles prompted us to directly compare patterns obtained with these and other antibodies to H4AcK16 and $H4Me_2K20$ throughout the mammalian cell cycle by both immunofluorescence and Western blotting.

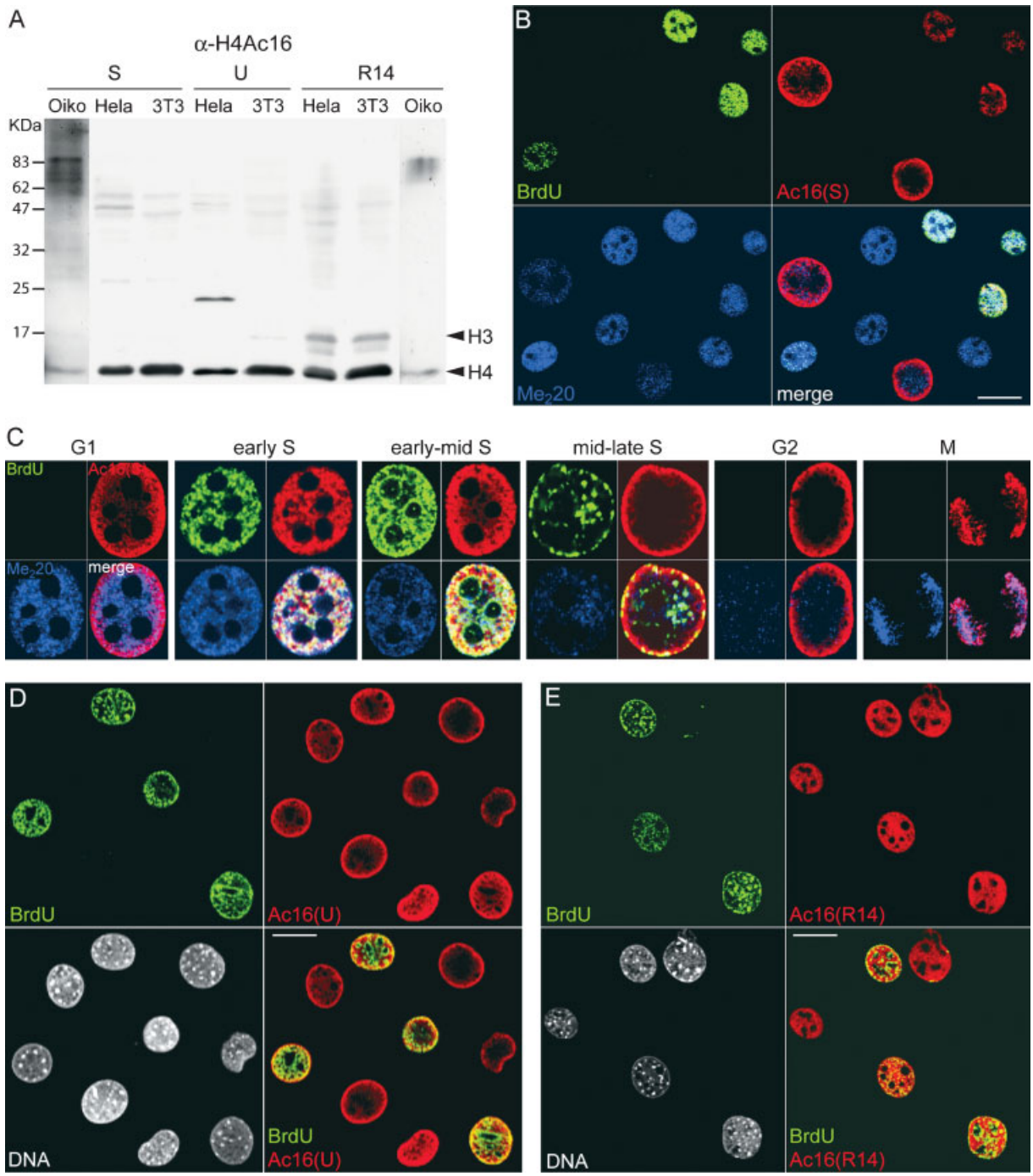

Fig. 4. Profiles and nuclear distribution of H4AcK16 and H4Me$_2$K20 throughout the mitotic cycle of cultured mammalian cells. **A**: Immunoblotting of extracts from *O. dioica* tadpoles, NIH3T3, and HeLa S3 cells with α-H4AcK16 S, U, and R14/16 antibodies. Molecular weight standards and migration of histones H3 and H4 are indicated. **B–E**: NIH3T3 fibroblasts were pulsed with BrdU and labeled with antibodies to BrdU (green), H4AcK16 (red), and either with the H4Me$_2$K20 MAb antibody (B, C; blue) or the DNA dye TO-PRO-3 (D, E; grayscale). Antibodies S, U, and R14/16 against H4AcK16 were used in (B)–(C), (D) and (E) respectively. C: Cell cycle dynamics of patterns obtained with H4AcK16 S and H4Me$_2$K20 MAb antibodies. Images for H4AcK16 S were collected with different acquisition settings in order to make the pattern visible in G1, early S, and M cells. All panels show single optical sections except that at the bottom right corner in (C) showing a projection of sections through a metaphase plate. **F–H**: HeLa S3 cells were synchronized at the G1/S-phase transition with a double thymidine block and released. F: Immunofluorescence patterns with serum H4AcK16 S on cells pulsed with BrdU for 10 min and immediately fixed at the indicated times after release. G: Immunoblots with antibodies to cyclin A and histone modifications as indicated on the right using whole cell extracts prepared at the times after release shown at the top along with corresponding cell cycle stages. H: Densitometric analysis of blots in (G). Time post release and corresponding cell cycle stages are indicated at the bottom of each plot. Blots were normalized directly by reprobing with antibodies to the H4 C-terminus and/or actin.

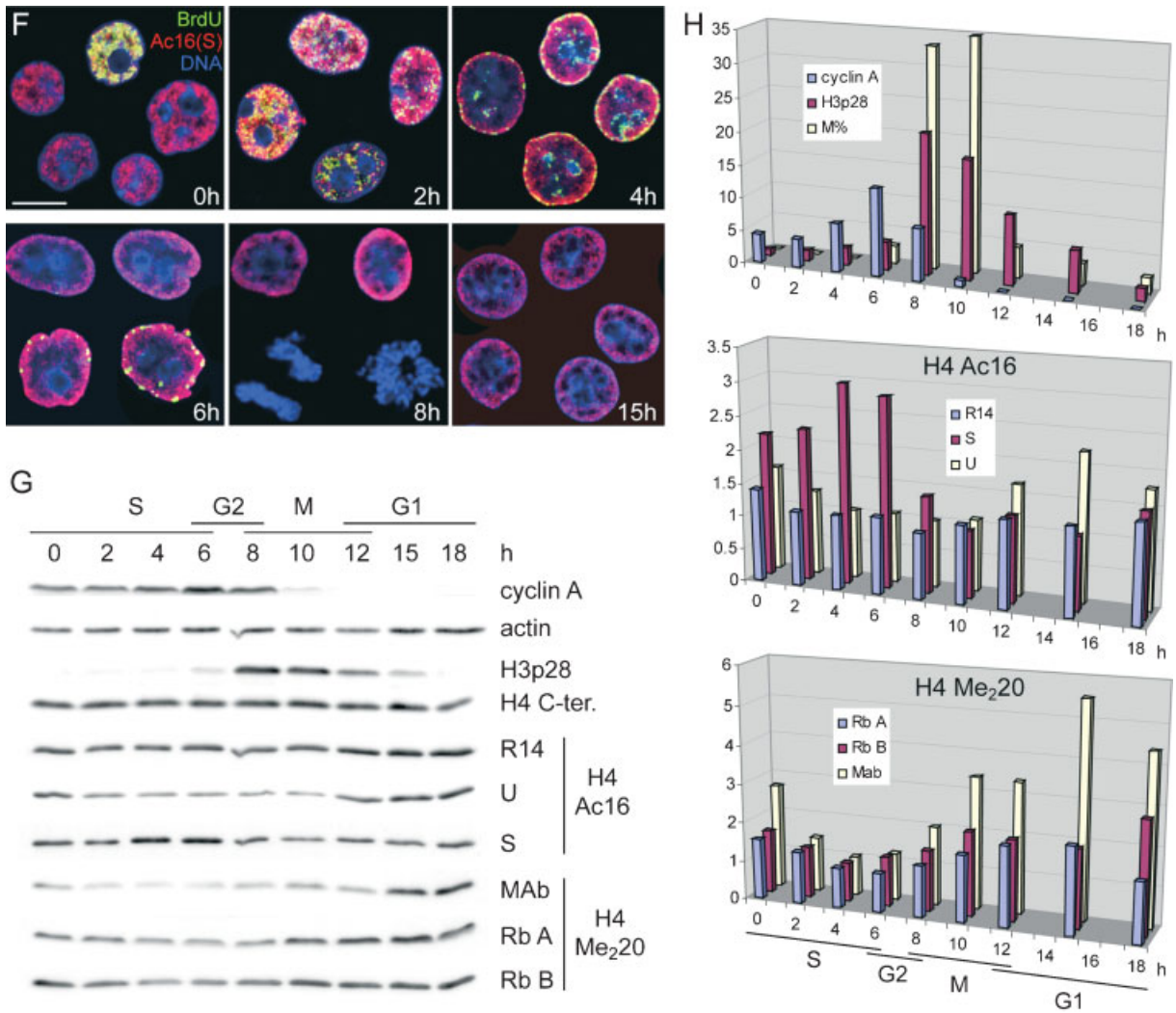

Fig. 4. (*Continued*)

Asynchronous cultures of mouse NIH3T3 and human HeLa S3 cells were pulsed with BrdU and then stained simultaneously with antibodies to BrdU, H4Me$_2$K20 (MAb), and serum H4AcK16 S (Fig. 4B,C and Supplementary Fig. 2). Alternatively, NIH3T3 cells were stained for BrdU and either sera H4AcK16 U [Suka et al., 2001], R14/16 (Fig. 4D,E, respectively), or α-H4Me$_2$K20 RbA (not shown). These experiments showed that nuclear signals for both antibodies to H4Me$_2$K20 decreased consistently and steadily from early to late S-phase (Fig. 4C). In contrast, α-H4AcK16 S signals increased during the same transition and surprisingly its nuclear pattern progressively changed from uniform throughout the euchromatic compartment in early S-phase to highly enriched at the nuclear periphery in late S-phase. These transitions were particularly evident when images were taken from the same field over a range of gain settings (Supplementary Fig. 2). Two combinations of α-H4AcK16 S and α-H4Me$_2$K20 patterns were observed among non-replicating (G-phase) cells. Both patterns showed enrichment of H4AcK16 signal at the nuclear periphery but one pattern with weaker H4AcK16 staining had correspondingly stronger H4Me$_2$K20 staining while in the other pattern, relative signal intensities were reversed. Among these G-phase cells, the subset with weak H4Me$_2$K20 signal showed an α-H4AcK16 S signal at the nuclear periphery of similar intensity to that in late S cells. The proportion of cells with each of the patterns suggested that they corresponded to G1 and G2 phases. This was confirmed by releasing NIH3T3 cells that had been blocked in mitosis with nocodazole (Supplementary Fig. 2C).

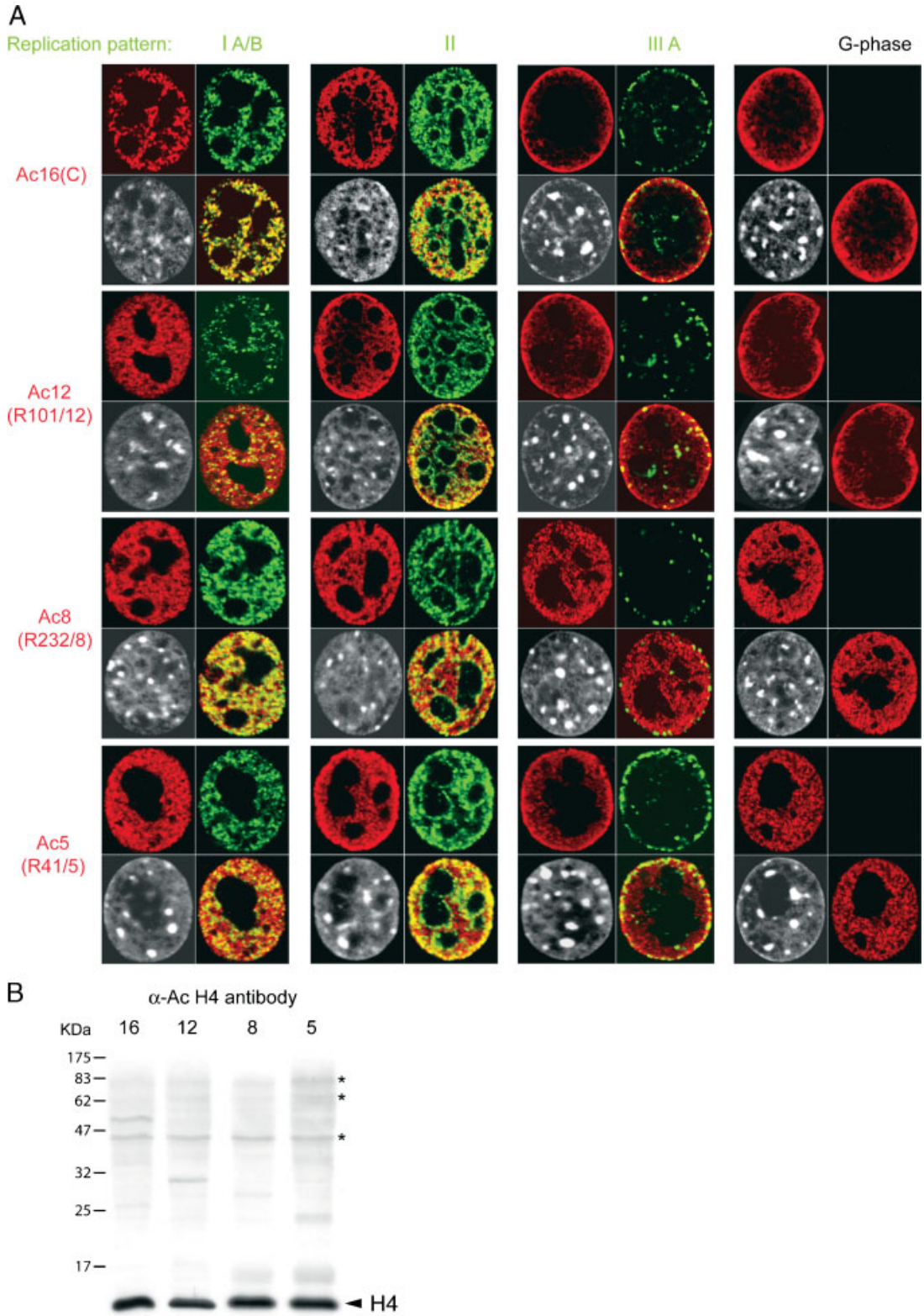

Fig. 5. Antibodies against H4AcK5, 12 and 16, but not 8, show similar nuclear distributions throughout the NIH3T3 cell cycle. **A**: Asynchronous NIH3T3 cells were pulsed with BrdU and immunolabeled with antibodies to BrdU (green) and H4 acetylated at either K5 (R41/5), 8 (R232/8), 12 (R101/12), or 16 (H4AcK16 S; all red) as indicated on the left. Grayscale panels show DNA staining with TO-PRO-3. Note that DNA density does not correlate with the peripheral staining of acetylated H4 at any cell cycle stage. Replication patterns were classified as previously [Dimitrova and Berezney, 2002]. **B**: Immunoblotting of NIH3T3 whole cell extracts with the antibodies used in (A). Molecular weight standards and position of histone H4 are indicated. Asterisks mark additional bands of similar molecular weight detected by all four antibodies.

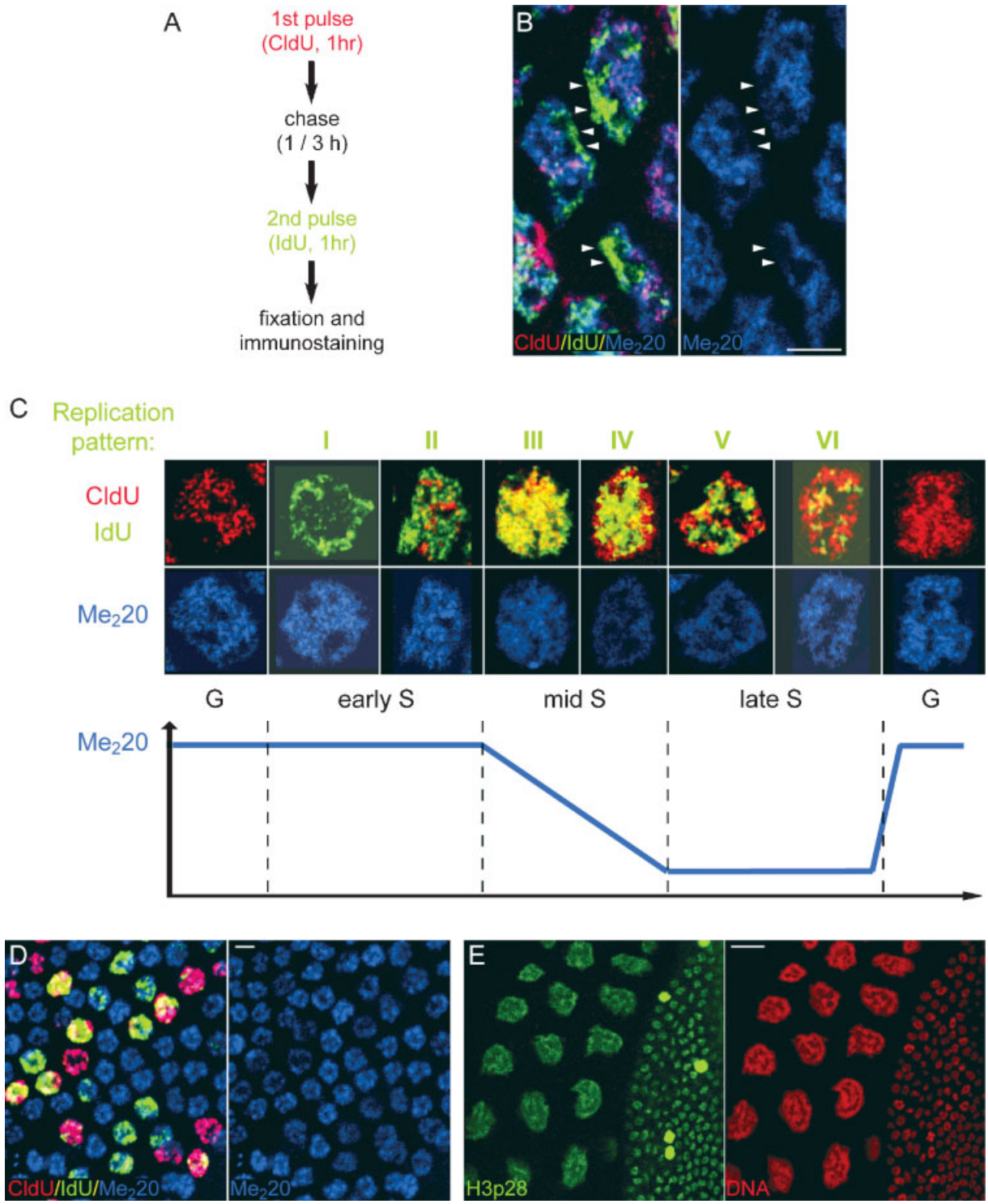

Fig. 6. Temporal sequence of DNA replication and H4Me$_2$K20 patterns during mitotic and endocycles of *Oikopleura dioica*. **A–D**: Stages of mitotic and endocycles in day 3 *O. dioica* tissues and associated levels of H4Me$_2$K20 were classified by sequential CldU (red) and IdU (green) pulse labeling and simultaneous labeling with antibody H4Me$_2$K20 RbA (blue). All images are single optical sections. A: Protocol: the chase time was 3 h in (B) and (C) and 1 h in (D). B: Endocycling cells in the anterior Fol region with arrowheads indicating regions of recent replication (IdU, green) where H4Me$_2$K20 was depleted. C: Temporal sequence of replication patterns and H4Me$_2$K20 levels throughout the endocycle. Dynamics of H4Me$_2$K20 levels are schematized below. D: Mitotically cycling cells of the intestinal endothelium of *O. dioica*. **E**: Endocycling cells in the posterior part of the oikoplastic epithelium (**right**) and proliferating cells of the intestinal endothelium (**left**) in an animal stained for H3Sp28 (green) and with DNA dye TO-PRO-3 (red). Note the similar basal H3Sp28 levels in endocycling and interphase endothelial cells as opposed to the very high levels in mitotic endothelial cells.

Under these conditions, the vast majority of non-replicating cells displayed a weak α-H4AcK16 S signal at the nuclear periphery and high levels of $H4Me_2K20$, defining the pattern for G1 cells. The temporal patterns of α-H4AcK16 S and $H4Me_2K20$ throughout the NIH3T3 cell cycle are recapitulated in Figure 4C. In order for the nuclear distribution of the α-H4AcK16 S signal to be discernible at all stages, images (red channel) were taken with different gain settings, therefore they do not reflect the relative intensity of the α-H4AcK16 S signal. Analysis of HeLa S3 cells synchronized by a double thymidine block gave similar cell cycle patterns with serum H4AcK16 S (Fig. 4F).

The α-H4AcK16 U antibody also revealed enriched staining at the nuclear periphery, but its signal distribution and intensity did not vary significantly at different cell cycle stages (Fig. 4D). Serum R14/16 exhibited different staining patterns of H4AcK16 compared to the other two antibodies directed against this epitope. Consistent with previous immunofluorescence data [Taddei et al., 1999] using this serum, uniform nuclear staining was observed at all cell cycle stages and similar to observations with this antibody in *O. dioica* cells, no substantial variation in staining intensity was detected with respect to cell cycle stage (Fig. 4E). To investigate whether polypeptides other than H4 might contribute to the immunofluorescence patterns observed using the different antibodies to H4AcK16, Western blotting was performed on total extracts of *O. dioica* tadpoles and asynchronous cultures of NIH3T3 and HeLa S3 cells (Fig. 4A). Each antibody cross-reacted with several polypeptides, some shared between mouse and human cells, but not present in *O. dioica*. In addition, some of the polypeptides recognized by sera H4AcK16 S and U had similar molecular weights in mammalian cells, raising the possibility that they may be responsible for the perinuclear staining. To investigate this, we tested the detergent solubility of antigens recognized by serum α-H4AcK16 S. As little as 0.1% NP-40 solubilized the majority of cross-reacting polypeptides detected by Western blotting, suggesting that they were not stable chromatin or nuclear matrix components (Supplementary Fig. 3A). However, the same treatment prior to fixation did not significantly affect the in situ enrichment of the immunofluorescence signal at the nuclear periphery (Supplementary Fig. 3B), indicating that detergent soluble cross-reacting polypeptides did not contribute substantially to the immunofluorescence pattern. This was also consistent with the fact that we were unable to immunoprecipitate any of the detergent soluble polypeptides with serum H4AcK16 S (not shown). Taken together, these results indicate that none of the cross-reacting bands on Western blots is likely to provide the epitopes recognized by the U and S antibodies at the nuclear periphery.

To quantify the levels of histone modification detected by the antibodies used in this study at different cell cycle stages, Western blotting was carried out on whole cell extracts from HeLa S3 cells synchronized by double thymidine block (Fig. 4G,H). Cyclin A and H3pS28 were used as markers of cell cycle progression. Each of the three antibodies to H4AcK16 yielded a substantially different cell cycle profile for this modification (Fig. 4H). These profiles were consistent with the respective signal levels observed by immunofluorescence at different cell cycle stages (Fig. 4B–F), while profiles obtained from cross-reacting polypeptides were not (not shown). These data suggested that the reactivity of the three antibodies directed against H4AcK16 is affected by undefined factors that are differentially modulated throughout the nuclear volume and, in the case of serum H4AcK16 S, in a cell cycle dependent manner. This complex reactivity does not allow confident determination of the cell cycle dynamics of the H4AcK16 epitope in this or previous studies. The three antibodies to $H4Me_2K20$ produced similar cell cycle profiles (Fig. 4H), with differences being in the amplitude of signal variations. These profiles were consistent with that of Rice et al. [2002], including the profile obtained for $H4Me_2K20$ RbB, previously published as an opposite profile [Fang et al., 2002]. No significant cross-reactions to polypeptides other than H4 (not shown) were observed with any of these antibodies and profiles obtained with antibodies $H4Me_2K20$ MAb and RbA matched the relative intensity of their immunofluorescence signals at different cell cycle stages (Fig. 4H and Supplementary Fig. 2).

Distributions of Histone H4 AcK5/K8/K12/K16 Throughout the Mammalian Cell Cycle

Enrichment of staining at the nuclear periphery has been previously reported using

antibodies to H4AcK5 and H2A-AcK5 in mammalian cultured cells [Taddei et al., 1999; Gilchrist et al., 2004] in both normally proliferating cells and those treated with the histone deacetylase (HDAC) inhibitor trichostatin A (TSA). To examine whether the nuclear distribution of acetylated isoforms of histone H4 at positions K5, K8, and K12 also varied as a function of cell cycle stage, NIH3T3 cells were pulsed with BrdU as above and labeled with antisera R41 to H4AcK5, R232 to H4AcK8 and R101 to H4AcK12 (Fig. 5A). Sera to both H4AcK5 and H4AcK12 yielded S-phase patterns similar to those observed for α-H4AcK16 S. The serum to H4AcK12 showed degrees of signal enrichment at the nuclear periphery from mid to late S-phase and in G-phase similar to that observed with serum H4AcK16 S, while this enrichment was less pronounced for H4AcK5 during S-phase and absent in the majority of G-phase cells. In contrast, H4AcK8 displayed no significant enrichment at the nuclear periphery at any cell cycle stage being consistently homogenously distributed throughout the euchromatic compartment and excluded from the perinuclear, perinucleolar, and satellite heterochromatin as reported previously [Sadoni et al., 1999]. Furthermore, in contrast to results obtained with serum α-H4AcK16 S, but similar to those with sera α-H4AcK16 U and R14/16, the signal intensity given by the sera to H4AcK5, 8 and 12 did not show any substantial or consistent variation among different cell cycle stages. These antibodies were also evaluated by Western blotting with whole cell extracts from exponentially growing NIH3T3 cells (Fig. 5B) and showed cross-reactions with several polypeptides some of which appeared to have similar molecular weights. Thus, a variety of sera to a panel of acetylated histone H4 N-terminal lysine residues recognized to different extents common antigens that are either enriched or more accessible at the nuclear periphery of mammalian cells in a cell cycle dependent fashion.

Similar $H4Me_2K20$ Dynamics in Mitotic and Endocycles of *O. dioica*

To establish a temporal sequence of distinct replication patterns and precise correlation between the cell cycle stage and nuclear levels of histone modifications, we adapted a procedure [Aten et al., 1992] for simultaneous labeling of DNA replicating at different times during S-phase. Day 3 animals were pulsed first with 5-clorodeoxyuridine (CldU) and then with 5-iododeoxyuridine (IdU) for 1 h each, with a 1 or 3 h chase between pulses (Fig. 6A). These samples were simultaneously evaluated with polyclonal antibodies to $H4Me_2K20$ (RbA) and monoclonal antibodies that selectively recognise the respective thymidine analogs (Fig. 6B–D). Comparison of CldU and IdU incorporation patterns defined six major replication patterns for oikoplastic cells and established their temporal sequence (Fig. 6C). The different replication patterns consistently correlated with distinct levels of $H4Me_2K20$, defining a profile throughout the endocycle for this modification (Fig. 6C).

Chromatin replicating at the beginning of S-phase was restricted to regions often positioned at the periphery of the nucleus (pattern I). This stage was characterized by overall sustained levels of $H4Me_2K20$, except for recently replicated chromatin where the modification was depleted. The difference in $H4Me_2K20$ signal intensity between recently replicated and non-replicated regions (Fig. 6B) was greater than expected for simple dilution of the histone modification due to DNA replication. Replication then spread to large regions of the nucleus, with IdU incorporation initially moderate (pattern II). At this stage, $H4Me_2K20$ levels remained essentially unaltered. In replication pattern III, the level of IdU incorporation was substantially higher, but the distribution of replicating chromatin changed very little, as reflected by extensive overlap of CldU and IdU incorporation patterns. Replication patterns IV and V were characterized by a progressive reduction in the overlap between CldU and IdU patterns, indicating that a chromatin fraction distinct from that replicated in the previous two stages had now been replicated. $H4Me_2K20$ levels declined progressively between replication patterns III and IV, while during the last part of S-phase (patterns V and VI) $H4Me_2K20$ attained basal levels. Surprisingly, the patterns of IdU incorporation (second pulse) at the end of S-phase resembled those for CldU at its beginning. Comparison of patterns corresponding to late S-, G- and early S-phase in experiments with 1 and 3 h chases was consistent with a rapid increase of $H4Me_2K20$ at the transition between S- and G-phases. Importantly, the staining intensity with antibodies to both H3pS28 (Fig. 6E) and 10 (not

shown) showed no significant variation in *O. dioica* endocycling cells remaining at low levels throughout. This indicated that not only morphological, but also molecular transitions associated with mitotic chromatin were absent in endocycling cells and that increased $H4Me_2K20$ at the late S- to G-phase transition was independent of mitotic events.

$H4Me_2K20$ cell cycle dynamics in mitotically dividing cells of *O. dioica* (Fig. 3) was confirmed and extended by analysis of the intestinal endothelium of day 3 animals double-pulsed with CldU and IdU (Fig. 6D). In this tissue, all major stages of the mitotic cycle were easily distinguished on the basis of CldU and IdU incorporation patterns. Incorporation of only IdU in restricted regions of the nucleus characterized early S-phase, as opposed to mid S-phase patterns with incorporation of IdU across most of the nucleus and late S-phase patterns showing incorporation of both CldU and IdU. Cells in early stages of mitosis showed only patchy CldU incorporation, while easily recognisable telophase nuclei did not incorporate any thymidine analog (not shown). Therefore, interphase nuclei showing incorporation of neither thymidine analog, and those that incorporated only CldU, identified G1 and G2 cells, respectively. In G1, $H4Me_2K20$ levels were high and then decreased substantially from early to late S, reaching basal levels in G2. Consistent with double staining for H3pS28 and $H4Me_2K20$ (Fig. 3C), levels of the latter modification increased at mitosis. Therefore, $H4Me_2K20$ levels in mitotically dividing *O. dioica* cells followed a very similar profile to that observed during the mitotic cycle of mammalian cells. Furthermore, in both mitotic and endocycling cells of *O. dioica*, $H4Me_2K20$ levels were high at the onset of S-phase and decreased during S-phase. Thus the major difference in $H4Me_2K20$ dynamics between the two types of cell cycle was that in the absence of mitosis $H4Me_2K20$ levels increased rapidly immediately at the S- to G-phase transition.

DISCUSSION

Detection and quantification of histone post-translational modifications rely on the use of highly specific antibodies. Even though some characterization of antibody specificity is routinely carried out [Turner et al., 1989; O'Neill and Turner, 1995; White et al., 1999], contrasting data have nonetheless been reported. This is particularly true of antibodies directed against acetylated lysine residues of the histone H4 N-terminal tail where inconsistencies in the degree of enrichment of these modifications at the nuclear periphery have been reported [Thompson et al., 1995; Worrad et al., 1995; Adenot et al., 1997; Stein et al., 1997; Taddei et al., 1999; Kim et al., 2003; Gilchrist et al., 2004]. In many of these studies, cell cycle stage was not considered, possibly accounting in part for the discrepancies. In the present work, enrichment at the nuclear periphery of mammalian cells was invariably observed at specific cell cycle stages with sera R41/5 (H4AcK5) and R101/12 (H4AcK12) (Fig. 5A). However, we found that different antibodies to H4AcK16 yielded striking inconsistencies in spatio-temporal cell cycle profiles as revealed both by immunofluorescence and immunoblotting. Two of the three antibodies displayed enriched staining at the periphery in mammalian nuclei, one of them in a cell cycle stage dependent fashion. Detergent extraction and immunoprecipitation experiments with antibody H4AcK16 S and data on defined cell cycle stages with sera H4AcK16 S and U suggest that the epitope primarily responsible for enrichment of the signal at the nuclear periphery may indeed be H4AcK16. Nonetheless, these results lend themselves to multiple interpretations of the reactivity of these antibodies, emphasizing that caution should be exercised in interpreting data obtained with them. This applies not only to immunofluorescence and immunoblotting, but also to chromatin immunoprecipitation procedures.

Territories of mammalian chromosomes with lower gene density have been shown to occupy more peripheral positions [Croft et al., 1999; Boyle et al., 2001; Cremer et al., 2001; Cremer et al., 2003], suggesting a radial organization in the nucleus. Thus, the possibility of a radial distribution of acetylated histone isoforms (or combination of histone modifications and/or other factors contributing to antibody reactivity) in mammalian nuclei is intriguing in this regard. In support of this possibility, MALDI-TOF mass spectrometric analysis of nuclear envelope-associated chromatin detected di- and tri-acetylated, but not mono-acetylated, histone H4 N-terminal peptides [Makatsori et al., 2004]. In addition, immunoprecipitation of native chromatin with the panel of antibodies

against acetylated histone H4 used in the present study showed that these modifications were enriched in non-coding SINE elements and either not significantly (AcK5, K8, and K12) or only slightly (AcK16) enriched in coding and adjacent regions relative to bulk chromatin [O'Neill and Turner, 1995; Johnson et al., 1998]. Further clarification is required to establish whether acetylated histone isoforms are indeed involved in a putative radial organization of chromatin in mammalian nuclei.

Endocycling Nuclei of *O. dioica* Exhibit Reduced Compartmentalization of Early and Late Replicating Chromatin Compared to Mammalian Cells

Early and late replication patterns were very similar during *O. dioica* endocycles. This contrasts the distinct distribution of early and late replicating chromatin in mammalian cells [O'Keefe et al., 1992; Dimitrova and Berezney, 2002] and suggests that early and late replicating sequences are less strictly compartmentalized in *O. dioica* endocycling nuclei. Interestingly, signal levels detected with serum H4AcK16 S showed cell cycle fluctuations in mitotic and endocycling cells of *O. dioica* similar to mammalian cells, but in contrast, enriched staining at the nuclear periphery was never observed with this antibody (Figs. 2 and 3) nor with sera R41/5 (H4AcK5) and R101/12 (H4AcK12) (not shown). Thus, though temporal fluctuations associated with the cell cycle occur in both *O. dioica* and mammalian cells, nuclear distributions of the immunofluorescent signals were disparate, also implying a different nuclear organization between *O. dioica* and mammalian cells.

$H4Me_2K20$ Displays Similar Dynamics in Mitotic and Endocycles

Of the two divergent mammalian cell cycle profiles previously described for $H4Me_2K20$, our results unequivocally support that proposed by Rice et al. [2002], showing an accumulation of this modification during mitosis and a decrease during S-phase. The reason for the accumulation of $H4Me_2K20$ during mitosis is unknown, but a recent study on human cells showed that levels of PR-Set7/Set8, the methyltransferase responsible for H4-K20 mono- and di-methylation, are controlled by the chromatin associated-factor HCF-1c and that PR-Set7/Set8, though not essential itself for proper cytokinesis, is involved in induction of cytokinesis defects upon depletion of HCF-1c [Julien and Herr, 2004]. In *O. dioica*, mitotically dividing cells showed similar temporal cell cycle dynamics of $H4Me_2K20$ to that observed in mammalian cells, suggesting a conservation of this role between urochordates and higher vertebrates. However, the observation that $H4Me_2K20$ also cycled in endoreduplicative cells of *O. dioica* showed that the dynamics of this modification is not strictly linked to constraints imposed by the mitotic phase of the cell cycle, as we observed no chromosomal transitions (condensation, accumulation of H3pS10/H3pS28) characteristic of mitotic events. This indicates other roles for this modification during G- and S-phase progression of the cell cycle.

ACKNOWLEDGMENTS

We thank B.M. Turner (University of Birmingham, UK) for his generous gifts of antibodies, G. Almouzni (Marie Curie Institute, France) for helpful discussions and Becky Upton for clarifying the origin of antibodies commercialized by Upstate. This work was supported by grants from the Norwegian Research Council and Ministry of Education, and by NFR Biotechnology grant 146653/431 (E.M.T.).

REFERENCES

Adenot PG, Mercier Y, Renard JP, Thompson EM. 1997. Differential H4 acetylation of paternal and maternal chromatin precedes DNA replication and differential transcriptional activity in pronuclei of 1-cell mouse embryos. Development 124:4615–4625.

Agalioti T, Chen G, Thanos D. 2002. Deciphering the transcriptional histone acetylation code for a human gene. Cell 111:381–392.

Aten JA, Bakker PJ, Stap J, Boschman GA, Veenhof CH. 1992. DNA double labelling with IdUrd and CldUrd for spatial and temporal analysis of cell proliferation and DNA replication. Histochem J 24:251–259.

Belyaev ND, Keohane AM, Turner BM. 1996. Histone H4 acetylation and replication timing in Chinese hamster chromosomes. Exp Cell Res 225:277–285.

Borun TW, Pearson D, Paik WK. 1972. Studies of histone methylation during the HeLa S-3 cell cycle. J Biol Chem 247:4288–4298.

Boyle S, Gilchrist S, Bridger JM, Mahy NL, Ellis JA, Bickmore WA. 2001. The spatial organization of human chromosomes within the nuclei of normal and emerin-mutant cells. Hum Mol Genet 10:211–219.

Braunstein M, Rose AB, Holmes SG, Allis CD, Broach JR. 1993. Transcriptional silencing in yeast is associated with reduced nucleosome acetylation. Genes Dev 7:592–604.

Braunstein M, Sobel RE, Allis CD, Turner BM, Broach JR. 1996. Efficient transcriptional silencing in *Saccharo-*

myces cerevisiae requires a heterochromatin histone acetylation pattern. Mol Cell Biol 16:4349–4356.
Chioda M, Spada F, Eskeland R, Thompson EM. 2004. Histone mRNAs do not accumulate during S phase of either mitotic or endoreduplicative cycles in the chordate *Oikopleura dioica*. Mol Cell Biol 24:5391–5403.
Clarke DJ, O'Neill LP, Turner BM. 1993. Selective use of H4 acetylation sites in the yeast *Saccharomyces cerevisiae*. Biochem J 294:557–561.
Cremer M, von Hase J, Volm T, Brero A, Kreth G, Walter J, Fischer C, Solovei I, Cremer C, Cremer T. 2001. Non-random radial higher-order chromatin arrangements in nuclei of diploid human cells. Chromosome Res 9:541–567.
Cremer M, Kupper K, Wagler B, Wizelman L, Hase Jv J, Weiland Y, Kreja L, Diebold J, Speicher MR, Cremer T. 2003. Inheritance of gene density-related higher order chromatin arrangements in normal and tumor cell nuclei. J Cell Biol 162:809–820.
Croft JA, Bridger JM, Boyle S, Perry P, Teague P, Bickmore WA. 1999. Differences in the localization and morphology of chromosomes in the human nucleus. J Cell Biol 145: 1119–1131.
Dimitrova DS, Berezney R. 2002. The spatio-temporal organization of DNA replication sites is identical in primary, immortalized and transformed mammalian cells. J Cell Sci 115:4037–4051.
Fang J, Feng Q, Ketel CS, Wang H, Cao R, Xia L, Erdjument-Bromage H, Tempst P, Simon JA, Zhang Y. 2002. Purification and functional characterization of SET8, a nucleosomal histone H4-lysine 20-specific methyltransferase. Curr Biol 12:1086–1099.
Forsberg EC, Bresnick EH. 2001. Histone acetylation beyond promoters: Long-range acetylation patterns in the chromatin world. Bioessays 23:820–830.
Ganot P, Thompson EM. 2002. Patterning through differential endoreduplication in epithelial organogenesis of the chordate, *Oikopleura dioica*. Dev Biol 252:59–71.
Gilchrist S, Gilbert N, Perry P, Bickmore WA. 2004. Nuclear organization of centromeric domains is not perturbed by inhibition of histone deacetylases. Chromosome Res 12:505–516.
Goto H, Tomono Y, Ajiro K, Kosako H, Fujita M, Sakurai M, Okawa K, Iwamatsu A, Okigaki T, Takahashi T, Inagaki M. 1999. Identification of a novel phosphorylation site on histone H3 coupled with mitotic chromosome condensation. J Biol Chem 274:25543–25549.
Goto H, Yasui Y, Nigg EA, Inagaki M. 2002. Aurora-B phosphorylates histone H3 at serine28 with regard to the mitotic chromosome condensation. Genes Cells 7:11–17.
Hendzel MJ, Wei Y, Mancini MA, Van Hooser A, Ranalli T, Brinkley BR, Bazett-Jones DP, Allis CD. 1997. Mitosis-specific phosphorylation of histone H3 initiates primarily within pericentromeric heterochromatin during G2 and spreads in an ordered fashion coincident with mitotic chromosome condensation. Chromosoma 106:348–360.
Jenuwein T, Allis CD. 2001. Translating the histone code. Science 293:1074–1080.
Jeppesen P, Turner BM. 1993. The inactive X chromosome in female mammals is distinguished by a lack of histone H4 acetylation, a cytogenetic marker for gene expression. Cell 74:281–289.
Johnson CA, O'Neill LP, Mitchell A, Turner BM. 1998. Distinctive patterns of histone H4 acetylation are associated with defined sequence elements within both heterochromatic and euchromatic regions of the human genome. Nucleic Acids Res 26:994–1001.
Julien E, Herr W. 2004. A switch in mitotic histone H4 lysine 20 methylation status is linked to M phase defects upon loss of HCF-1. Mol Cell 14:713–725.
Kim JM, Liu H, Tazaki M, Nagata M, Aoki F. 2003. Changes in histone acetylation during mouse oocyte meiosis. J Cell Biol 162:37–46.
Kurdistani SK, Grunstein M. 2003. Histone acetylation and deacetylation in yeast. Nat Rev Mol Cell Biol 4:276–284.
Kurdistani SK, Tavazoie S, Grunstein M. 2004. Mapping global histone acetylation patterns to gene expression. Cell 117:721–733.
Lachner M, O'Sullivan RJ, Jenuwein T. 2003. An epigenetic road map for histone lysine methylation. J Cell Sci 116:2117–2124.
Makatsori D, Kourmouli N, Polioudaki H, Shultz LD, McLean K, Theodoropoulos PA, Singh PB, Georgatos SD. 2004. The inner nuclear membrane protein lamin B receptor forms distinct microdomains and links epigenetically marked chromatin to the nuclear envelope. J Biol Chem 279:25567–25573.
Nishioka K, Rice JC, Sarma K, Erdjument-Bromage H, Werner J, Wang Y, Chuikov S, Valenzuela P, Tempst P, Steward R, Lis JT, Allis CD, Reinberg D. 2002. PR-Set7 is a nucleosome-specific methyltransferase that modifies lysine 20 of histone H4 and is associated with silent chromatin. Mol Cell 9:1201–1213.
O'Keefe RT, Henderson SC, Spector DL. 1992. Dynamic organization of DNA replication in mammalian cell nuclei: Spatially and temporally defined replication of chromosome-specific alpha-satellite DNA sequences. J Cell Biol 116:1095–1110.
O'Neill LP, Turner BM. 1995. Histone H4 acetylation distinguishes coding regions of the human genome from heterochromatin in a differentiation-dependent but transcription-independent manner. Embo J 14:3946–3957.
Rice JC, Nishioka K, Sarma K, Steward R, Reinberg D, Allis CD. 2002. Mitotic-specific methylation of histone H4 Lys 20 follows increased PR-Set7 expression and its localization to mitotic chromosomes. Genes Dev 16:2225–2230.
Sadoni N, Langer S, Fauth C, Bernardi G, Cremer T, Turner BM, Zink D. 1999. Nuclear organization of mammalian genomes. Polar chromosome territories build up functionally distinct higher order compartments. J Cell Biol 146:1211–1226.
Schotta G, Lachner M, Sarma K, Ebert A, Sengupta R, Reuter G, Reinberg D, Jenuwein T. 2004. A silencing pathway to induce H3-K9 and H4-K20 trimethylation at constitutive heterochromatin. Genes Dev 18:1251–1262.
Spada F, Vincent M, Thompson EM. 2005. Plasticity of histone modifications across the invertebrate to vertebrate transition: Histone H3 lysine 4 trimethylation in heterochromatin. Chromosome Res 13:57–72.
Stein P, Worrad DM, Belyaev ND, Turner BM, Schultz RM. 1997. Stage-dependent redistributions of acetylated histones in nuclei of the early preimplantation mouse embryo. Mol Reprod Dev 47:421–429.
Suka N, Suka Y, Carmen AA, Wu J, Grunstein M. 2001. Highly specific antibodies determine histone acetylation site usage in yeast heterochromatin and euchromatin. Mol Cell 8:473–479.

Taddei A, Roche D, Sibarita JB, Turner BM, Almouzni G. 1999. Duplication and maintenance of heterochromatin domains. J Cell Biol 147:1153–1166.

Thompson EM, Legouy E, Christians E, Renard JP. 1995. Progressive maturation of chromatin structure regulates HSP70.1 gene expression in the preimplantation mouse embryo. Development 121:3425–3437.

Thorne AW, Kmiciek D, Mitchelson K, Sautiere P, Crane-Robinson C. 1990. Patterns of histone acetylation. Eur J Biochem 193:701–713.

Turner BM. 2000. Histone acetylation and an epigenetic code. Bioessays 22:836–845.

Turner BM. 2002. Cellular memory and the histone code. Cell 111:285–291.

Turner BM, O'Neill LP, Allan IM. 1989. Histone H4 acetylation in human cells. Frequency of acetylation at different sites defined by immunolabeling with site-specific antibodies. FEBS Lett 253:141–145.

Waterborg JH. 1992. Identification of five sites of acetylation in alfalfa histone H4. Biochemistry 31:6211–6219.

White DA, Belyaev ND, Turner BM. 1999. Preparation of site-specific antibodies to acetylated histones. Methods 19:417–424.

Worrad DM, Turner BM, Schultz RM. 1995. Temporally restricted spatial localization of acetylated isoforms of histone H4 and RNA polymerase II in the 2-cell mouse embryo. Development 121:2949–2959.

Zhang K, Williams KE, Huang L, Yau P, Siino JS, Bradbury EM, Jones PR, Minch MJ, Burlingame AL. 2002. Histone acetylation and deacetylation: Identification of acetylation and methylation sites of HeLa histone H4 by mass spectrometry. Mol Cell Proteomics 1:500–508.